

Nonreciprocal photon blockade in a spinning microwave magnomechanical system through kerr-magnon and optical parametric amplifier

S. K. Singh,¹ Mohamed Amazioug,^{2,*} Jia-Xin Peng,³ and Mohammad Khalid^{4,5}

¹*Department of Physics, Akal University, Talwandi Sabo, Bathinda, Punjab 151302, India*

²*LPTHE, Department of Physics, Faculty of sciences, Ibnou Zohr University, Agadir, Morocco*

³*School of Physical Science and Technology, Nantong University, Nantong 226019, People's Republic of China*

⁴*Sunway Centre for Electrochemical Energy and Sustainable Technology (SCEEST),*

School of Engineering and Technology, Sunway University, No. 5 Jalan Universiti,

Bandar Sunway, 47500, Petaling Jaya, Selangor, Malaysia

⁵*University Centre for Research and Development, Chandigarh University, Mohali, Punjab, 140413, India*

Unconventional quantum antibunching, arising from quantum interference effects, represents a notable form of quantum correlation that has attracted significant attention for its ability to generate high-quality single-quantum sources. In this work, we propose a scheme to achieve and actively control strong photon blockade in a spinning microwave magnomechanical system by leveraging the combined nonlinear effects of Kerr-induced magnon interactions and an optical parametric amplifier. By exploiting the Sagnac-Fizeau shift, we establish nonreciprocal photon blockade and verify this effect through a combination of analytical modelling and numerical simulations. To gain intuitive insight into the underlying nonreciprocity, we approximate the equal-time second-order correlation function using the analytical solution of the Schrödinger equation. This analytical result is then compared with the full numerical solution derived from the Lindblad master equation. The influences of thermal noise, the probe field amplitude, and the magnetic-dipole coupling strength are investigated within the constraints of the weak-coupling regime. The system's nonclassicality is characterized using the Mandel parameter, complemented by an analysis of the time evolution of the second-order correlation function. Our work provides a pathway for realizing nonreciprocal photon blockade in a nonlinear spinning microwave magnomechanical system.

I. INTRODUCTION

The photon blockade (PB) effect, a key mechanism for single-photon generation, arises when the presence of one photon in a nonlinear medium prevents the entry of another. It plays a pivotal role in quantum metrology [1] and quantum information processing [2–4], enabling precise measurements and reliable single-photon sources for quantum communication and computing. Photon blockade (PB) is mainly classified into two categories. The first is conventional photon blockade (CPB), which originates from the anharmonicity of energy levels and requires strong nonlinear interactions to suppress multi-photon excitations. The second is unconventional photon blockade (UPB), which relies on destructive quantum interference between different excitation pathways, allowing photon blockade to occur even in systems with weak nonlinearities. Experimental realizations of CPB have been reported in systems like photonic crystals with quantum dots [5], cavity QED [6–10], and circuit QED [11, 12]. In contrast, UPB has been demonstrated in circuit QED [13] and coupled quantum-dot-cavity systems [14].

Optical reciprocity requires a system to exhibit exchange symmetry, meaning the transmission response remains the same when the input and output ports are interchanged. Optical nonreciprocal devices, such as optical isolators [15, 16] and circulators [17], break this symmetry, allowing light to travel in only one direction. This one-way behavior helps protect light sources from unwanted back reflections and noise, making these devices vital for applications like invisible sensing [18] and backaction-immune optical communications [19] as well as enabled effects like nonreciprocal entanglement [20–23], phonon lasing [24, 25], slow light [47, 48], and optical solitons [49]. In 2018, nonreciprocal PB was theoretically proposed in a spinning Kerr resonator [50], followed by its realization in various platforms which includes nonlinear cavities [51–53], optomechanical systems [54–56], atom-cavity systems [57–60], and cavity optomagnonics [61]. Experimental implementations based on cavity optomechanical systems face experimental challenges as because of requirement of maintaining a stable inter-cavity coupling.

Spinning microwave magnomechanical systems may offer a compelling alternative as such systems benefit from strong photon-magnon coupling via Kittel modes in YIG spheres [26, 62–65] and tunable magnon frequencies via external magnetic fields. Moreover, the magnetostrictive interaction provides controllable coupling with phonons [27–29, 66, 67], and superconducting qubits [30, 31]. Nonreciprocal quantum phenomena such as entanglement [68] and phonon lasing [25] have

*m.amazioug@uiz.ac.ma

recently been explored in these platforms. These developments motivate the study of nonreciprocal UPB in spinning microwave magnomechanical systems. With the help of well known Sagnac effect and quantum interference, it might also becomes possible to achieve direction-dependent photon statistics, laying the foundation for tunable nonreciprocal single-photon sources in cavity magnomechanical systems. Consequently, magnomechanics presents an exciting platform for exploring various quantum phenomena, such as quantum correlations [32–35], cooling [36], non-reciprocity (including photon and magnon blockade) [37–42], and thermodynamics [43, 44].

With advancements in the quality and performance of nonlinear optical crystals, optical parametric amplifiers (OPAs), including both degenerate and nondegenerate configurations, have become essential tools for generating high-purity squeezed and entangled quantum states [69–72]. Interference effects in the quantum fluctuations of OPA outputs were analysed, and it was shown that such interference phenomena can be precisely controlled by tailoring the squeezing properties of the input field [70]. The generation of broadband entangled light via cascaded nondegenerate OPAs was reported, and its applicability to broadband quantum teleportation was discussed, demonstrating strong potential for continuous-variable quantum information processing [71]. More recently, enhancement of entanglement has been investigated through the implementation of nondegenerate OPAs [73, 74, 76]. It was theoretically demonstrated that the correlation strength of pre-existing entangled beams can be significantly improved by incorporating a nondegenerate OPA inside an optical cavity [73], while experimental studies verified that both the degree and tunability of entanglement can be effectively enhanced using nondegenerate OPA-based architectures [74, 76], thereby providing a promising pathway for advanced quantum resource engineering in photonic platforms.

In this work, we propose a scheme to investigate nonreciprocal photon blockade effect in a spinning microwave magnomechanical system using kerr-magnon and optical parametric amplifier under the weak driving limit in terms of the second-order correlation function. A strong photon blockade effect is achieved analytically and numerically through precise control of the nonlinear parameter and utilizing feasible parameters. Moreover, we study the impact of thermal effect, the amplitude of a probe field, and the magnetic-dipole coupling strength on the realization of a photon blockade. Also, we employ the Mandel parameter to harnessing the nonclassicality in the system. Besides, we study the time-delay second-order correlation function and power spectrum.

This paper is organized as follows: in section II, we investigate a spinning microwave magnomechanical system with kerr-magnon and optical parametric amplifier and give its Hamiltonian under weak coupling. In section III, we employ the second-order correlation function to characterize nonreciprocal photon blockade under optimal parameters with analytically and numerically approach. The results and discussions are studied in section IV. Finally, a conclusion is given in section V.

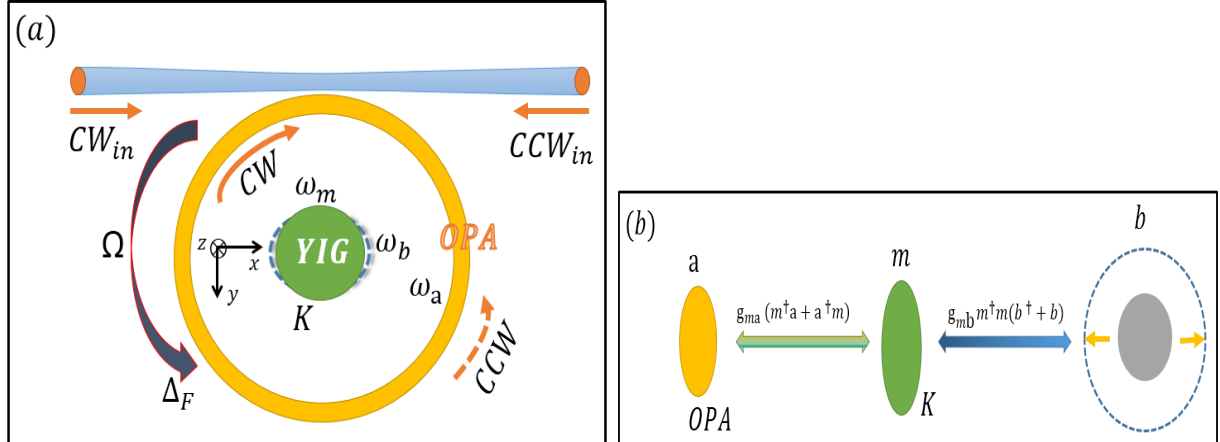


FIG. 1: (a) The panel illustrates a spinning microwave magnetomechanical system, incorporating magnon squeezing. A spinning optical resonator (mode a) is driven from either the left or the right side, generating a Sagnac-Fizeau shift (Δ_F), where the sign corresponds to the drive direction ($\Delta_F \gtrless 0$). A bias magnetic field H fully magnetizes the YIG sphere, which supports the magnon mode (m) and the phonon mode (b). Crucially, the YIG sphere's rotation at angular frequency Δ_B induces an emergent magnetic field \mathbf{H} , which shifts the magnon mode frequency. (b) photons in the cavity couple to the magnons via the magnetic dipole interaction, while magnons couple to the phonons through the magnetostrictive effect, which functions similarly to radiation pressure.

II. MODEL HAMILTONIAN

We consider a spinning cavity magnomechanical system, where the resonant frequency of the counter propagating modes experiences a Sagnac-Fizeau shift given by

$$\Delta_F = \pm \Omega \frac{nr\omega_a}{c} \left(1 - \frac{1}{n^2} - \frac{\lambda}{n} \frac{dn}{d\lambda} \right), \quad (1)$$

Here Ω is the angular velocity, n and r are the refractive index and radius of the microwave resonator, c is the speed of light in vacuum, λ is the wavelength, and ω_a is the resonant frequency of the nonspinning cavity. The total Hamiltonian in a rotating frame with respect to the driving frequency ω_d is

$$\mathcal{H}_1 = \mathcal{H}_0 + \mathcal{H}_I + \mathcal{H}_K + \mathcal{H}_{OPA} + \mathcal{H}_d, \quad (2)$$

where the free Hamiltonian is

$$\mathcal{H}_0 = (\Delta_a + \Delta_F)a^\dagger a + \Delta_m m^\dagger m + \omega_b b^\dagger b, \quad (3)$$

with $a^\dagger(a)$, $m^\dagger(m)$, $b^\dagger(b)$ being the creation (annihilation) operators for microwave cavity, magnon, and phonon modes, respectively. $\Delta_a = \omega_a - \omega_d$ and $\Delta_m = \omega_m - \omega_d$. The interaction Hamiltonian is

$$\mathcal{H}_I = J(a^\dagger m + a m^\dagger) - g m^\dagger m (b^\dagger + b), \quad (4)$$

where J is the magnon-photon coupling strength and g is the magnon-phonon coupling strength. The Hamiltonian of kerr, writes as

$$\mathcal{H}_K = K_0 (m^\dagger m)^2, \quad (5)$$

and Hamiltonian of the parametric amplifier

$$\mathcal{H}_{OPA} = i\Lambda[(a^\dagger)^2 e^\beta - a^2 e^{-\beta}], \quad (6)$$

where Λ is the squeezing parameter, quantifying the degree of squeezing, and β is the squeezing angle (phase). The driving term is given by

$$\mathcal{H}_d = \varepsilon(a^\dagger + a), \quad (7)$$

with ε being the driving amplitude. Applying a canonical transformation and assuming weak coupling $g/\omega_b \ll 1$, the effective Hamiltonian becomes

$$\mathcal{H}_2 = (\Delta_a + \Delta_F)a^\dagger a + \Delta_m m^\dagger m + \omega_b b^\dagger b + K(m^\dagger m)^2 + J(a^\dagger m + a m^\dagger) + i\Lambda[(a^\dagger)^2 e^\beta - a^2 e^{-\beta}] + \varepsilon(a^\dagger + a), \quad (8)$$

where the Kerr-type nonlinear strength is $K = K_0 - \frac{g^2}{\omega_b}$. Neglecting the decoupled phonon term, the reduced Hamiltonian is

$$\mathcal{H} = (\Delta_a + \Delta_F)a^\dagger a + \Delta_m m^\dagger m + K(m^\dagger m)^2 + J(a^\dagger m + a m^\dagger) + i\Lambda[(a^\dagger)^2 e^\beta - a^2 e^{-\beta}] + \varepsilon(a^\dagger + a), \quad (9)$$

with the mode assignment depending on the driving direction:

$$\begin{cases} a = a_{\text{cw}}, & \text{Left input (CW mode)} \\ a = a_{\text{ccw}}, & \text{Right input (CCW mode)} \end{cases} \quad (10)$$

The Hamiltonian of non-Hermitian system writes as

$$\mathcal{H} = (\Delta_a + \Delta_F - i\frac{\gamma_a}{2})a^\dagger a + (\Delta_m - i\frac{\gamma_m}{2})m^\dagger m + K(m^\dagger m)^2 + J(a^\dagger m + a m^\dagger) + i\Lambda[(a^\dagger)^2 e^\beta - a^2 e^{-\beta}] + \varepsilon(m^\dagger + m), \quad (11)$$

III. NONRECIPROCAL PHOTON BLOCKADE

In this section, we concentrate on the analytical solution of the non-Hermitian Schrödinger equation as well as numerical solution using Master equation. In addition, we talk about the weak coupling regime's ability to realize a strong photon blockade ($g_{mb} \ll \omega_b$). By solving the Schrödinger equation $i\partial_t|\Psi(t)\rangle = \mathcal{H}_2|\Psi(t)\rangle$ in the weak driving limit, where $|\Psi(t)\rangle$ represents the system's state, we obtain the analytical expression for the correlation function. This solution is found by truncating the Hilbert space to the low-excitation subspace $\mathcal{D} = \{|m, n\rangle \mid m + n \leq 2\}$, encompassing states with up to two total excitations. In the bare-state basis $|m, n\rangle$ (where m and n are the magnon and photon numbers in the cavity), the system state within the $m + n \leq 2$ low-excitation subspace is written as

$$|\Psi(t)\rangle = \sum_{m,n}^{m+n \leq 2} C_{mn}(t)|m, n\rangle \quad (12)$$

where, $C_{mn}(t)$ denotes the time-dependent amplitude of the state $|m, n\rangle$. The probability amplitudes $C_{mn}(t)$ satisfy a set of linear differential equations derived from the Schrödinger equation

$$i\partial_t C_{00} = \mathcal{E}C_{01} - i\sqrt{2}\Lambda e^{-i\beta}C_{02}, \quad (13)$$

$$i\partial_t C_{10} = \mathcal{E}C_{11} + (\Delta'_m + K)C_{10} + JC_{01}, \quad (14)$$

$$i\partial_t C_{01} = JC_{10} + (\Delta'_c + \Delta_F)C_{01} + \mathcal{E}C_{00} + \sqrt{2}\mathcal{E}C_{02}, \quad (15)$$

$$i\partial_t C_{11} = \sqrt{2}JC_{20} + \mathcal{E}C_{10} + (\Delta'_c + \Delta_F + \Delta'_m + K)C_{11} + \sqrt{2}JC_{02}, \quad (16)$$

$$i\partial_t C_{02} = \sqrt{2}JC_{11} + 2(\Delta'_c + \Delta_F)C_{02} + \sqrt{2}\mathcal{E}C_{01} + i\sqrt{2}\Lambda e^{i\beta}C_{00}, \quad (17)$$

$$i\partial_t C_{20} = 2(\Delta'_m + 2K)C_{20} + \sqrt{2}JC_{11}, \quad (18)$$

where $\Delta'_a = \Delta_a - i\gamma_a/2$ and $\Delta'_m = \Delta_m - i\gamma_m/2$. The equations (13)-(18) are analytically solvable, yielding the dynamical state. For the steady state, we solve $\partial_t C_{mn} = 0$. In the case of weak coupling interaction, this equation is simplified using appropriate approximations, for instance, by ignoring higher-order terms. For simplicity, we set, $\Delta_a = \Delta_m = \Delta$ and $\gamma_a = \gamma_m = \gamma$. In the weak driving limit ($\mathcal{E} \ll \gamma$), the probability amplitudes satisfy the hierarchy $|C_{00}| \simeq 1 \gg |C_{01}|, |C_{10}| \gg |C_{11}|, |C_{02}|, |C_{20}|$.

$$C_{01} = -\frac{(K + \Delta'_m)\epsilon}{-J^2 + K\Delta'_a + \Delta'_a\Delta'_m + K\Delta_F + \Delta'_m\Delta_F}, \quad (19)$$

The explicit expression of C_{02} is cumbersome. The Photon blockade is quantified by the steady-state second-order correlation function $g_a^{(2)}(0)$, given by

$$g_a^{(2)}(0) = \frac{2|C_{02}|^2}{|C_{01}|^4} = \frac{\text{Tr}[a^\dagger a^\dagger a a \varrho_s]}{\text{Tr}[a^\dagger a \varrho_s]}. \quad (20)$$

The statistical properties of photon is characterized by the equal-time second-order correlation function $g_a^{(2)}(0)$. Specifically, $g_a^{(2)}(0) > 1$ signifies bunching, while $g_a^{(2)}(0) < 1$ indicates antibunching. Perfect photon blockade occurs when $g_a^{(2)}(0) = 0$, with $g_a^{(2)}(0) = 0$ corresponds to strong photon blockade. This property is numerically investigated by solving the Master equation, which has the following expression

$$\partial_t \varrho = -i[\mathcal{H}_1, \varrho] + \frac{\gamma}{2}L_a(\varrho) + \frac{\gamma}{2}[m_{th} + 1]L_m(\varrho) + \frac{\gamma}{2}m_{th}L_{m^\dagger}(\varrho) \quad (21)$$

where the terms are defined as follows: \mathcal{H}_1 is the Hamiltonian from Equation (2); L_a and L_m are the Lindblad superoperators given by $L_a(\varrho) = 2a\varrho a^\dagger - \{a^\dagger a, \varrho\}$ and $L_m(\varrho) = 2m\varrho m^\dagger - \{m^\dagger m, \varrho\}$ for the optical a and magnon m modes, respectively; and γ is the decay rate of the magnon m mode. In steady state, the density matrix ϱ is characterized by $\partial_t \varrho = 0$.

IV. RESULTS AND DISCUSSIONS

The achieved photon blockade effect belongs to the UCPB (destructive quantum interference). Here we employ the parameters value considered [45]: $\gamma/2\pi = 0.55 \times 10^6$ Hz, $\omega_b/2\pi = 11.0308 \times 10^6$ Hz, $E = 0.005\gamma$, $J/2\pi = 7.37 \times 10^6$ Hz, and $K = 0.1\gamma$ [46]. The Sagnac-Fizeau shift Δ_F as a function angular velocity Ω , with the refractive index $n = 1.4$, the resonator's radius $r = 30\mu\text{m}$, the vacuum wavelength of light $\lambda = 1550\text{nm}$, and the vacuum speed of light $c = 3 \times 10^8\text{m/s}$ [75]. The optimal parameter pairs λ and Δ can be obtained together with the other fixed parameters. Beside, the real solution of the optimal parameter pairs value:

* $\Delta_F = 0.5\gamma$: for photon blockade $\{\Delta_{\text{opt}} = -0.684495\omega_b, \lambda_{\text{opt}} = 2.46157 \times 10^{-6}\omega_b\}; \{\Delta_{\text{opt}} = 0.654639\omega_b, \lambda_{\text{opt}} = 2.45563 \times 10^{-6}\omega_b\}$.

* $\Delta_F = -0.5\gamma$: for photon blockade $\{\Delta_{\text{opt}} = 0.679535\omega_b, \lambda_{\text{opt}} = 2.46105 \times 10^{-6}\omega_b\}; \{\Delta_{\text{opt}} = -0.659796\omega_b, \lambda_{\text{opt}} = 2.47275 \times 10^{-6}\omega_b\}$.

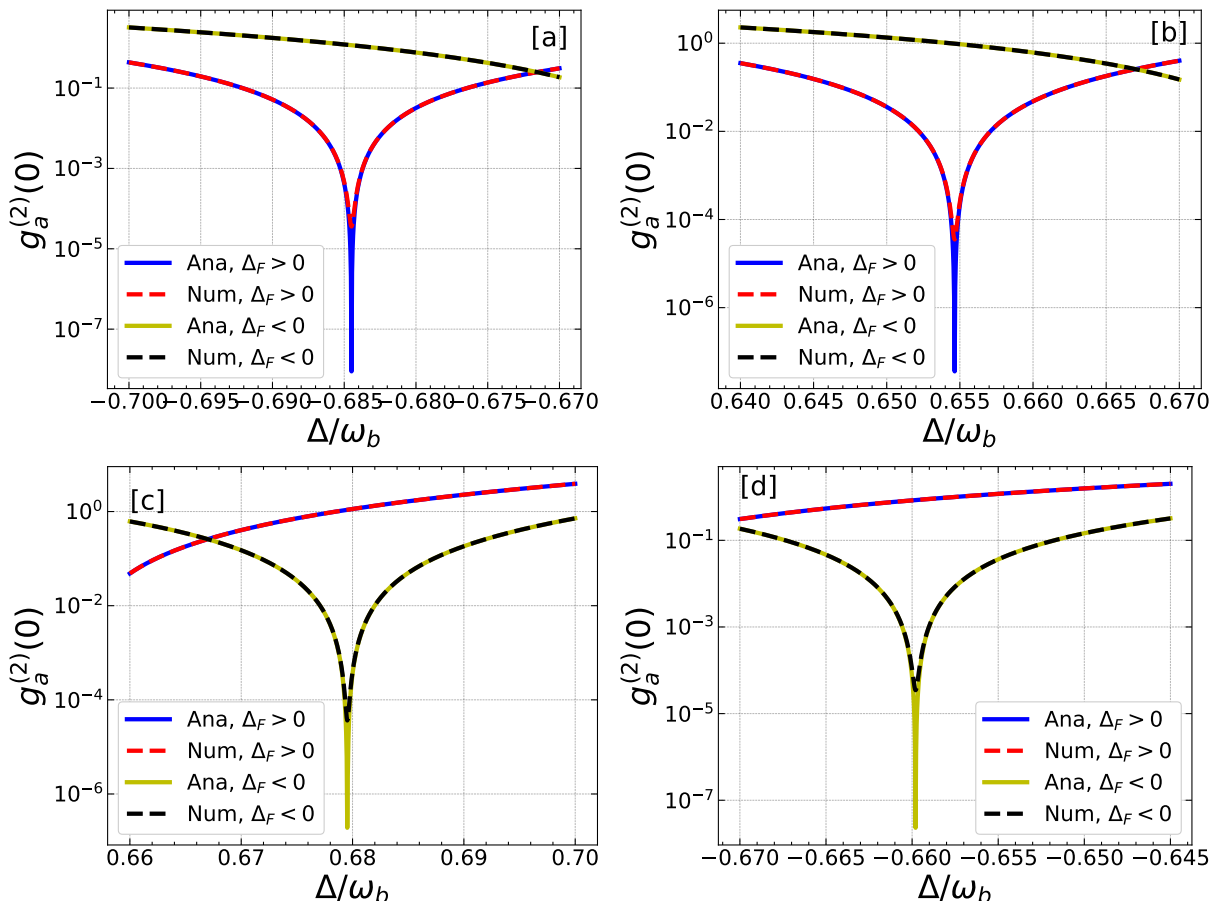


FIG. 2: Plot numerical (Num) and analytical (Ana) of the equal-time second-order correlation function $g_a^{(2)}(0)$ versus the normalized detuning Δ/ω_b for $|\Delta_F| = 0.5\gamma$ with $\lambda = \lambda_{\text{opt}} \approx (2.46, 2.46, 2.46 \text{ and } 2.47) \times 10^{-6}\omega_b$ in (a), (b), (c) and (d), respectively. See the text for value of other parameters.

Figure 2 compares the analytical (Ana) and numerical (Num) results of the equal-time second-order correlation function $g_a^{(2)}(0)$ as a function of the normalized detuning Δ/ω_b for $|\Delta_F| = 0.5\gamma$. The achieved photon blockade effect due to CW or CCW mode belong to the UCPB (destructive quantum interference). Each panel corresponds to one of the four real optimal parameter pairs $(\Delta_{\text{opt}}, \lambda_{\text{opt}})$: (a) $\Delta_{\text{opt}} = -0.684495\omega_b, \lambda_{\text{opt}} = 2.46157 \times 10^{-6}\omega_b$; (b) $\Delta_{\text{opt}} = 0.654639\omega_b, \lambda_{\text{opt}} = 2.45563 \times 10^{-6}\omega_b$; (c) $\Delta_{\text{opt}} = 0.679535\omega_b, \lambda_{\text{opt}} = 2.46105 \times 10^{-6}\omega_b$; and (d) $\Delta_{\text{opt}} = -0.659796\omega_b, \lambda_{\text{opt}} = 2.47275 \times 10^{-6}\omega_b$. Panels (a)–(b) correspond to $\Delta_F = 0.5\gamma$, where the clockwise (CW) mode is driven, whereas panels (c)–(d) correspond to $\Delta_F = -0.5\gamma$, where the counterclockwise (CCW) mode is driven.

For $\Delta_F = 0.5\gamma$, the CW-driven cavity clearly exhibits strong photon antibunching at the optimal detunings $\Delta_{\text{opt}} = -0.684495\omega_b$ and $\Delta_{\text{opt}} = 0.654639\omega_b$, where $g_a^{(2)}(0)$ reaches values as low as 10^{-5} . In contrast, the CCW response un-

der the same conditions displays photon bunching ($g_a^{(2)}(0) > 1$), confirming the nonreciprocal nature of the unconventional photon blockade (UPB). When the rotation direction is reversed ($\Delta_F = -0.5\gamma$), the behaviour interchanges: the CCW-driven mode shows deep antibunching at $\Delta_{\text{opt}} = 0.679535\omega_b$ and $\Delta_{\text{opt}} = -0.659796\omega_b$, whereas the CW-driven mode becomes bunched. The excellent agreement between the analytical and numerical results across all four cases validates the accuracy of the truncated-state analytical model. These results collectively confirm that photon statistics in the spinning magnomechanical cavity are strongly direction-dependent, arising from destructive quantum interference between distinct excitation pathways. This interference effectively suppresses multiphoton transitions, producing single-photon emission with extremely low $g_a^{(2)}(0)$ values. Hence, the proposed spinning microwave magnomechanical system acts as a highly tunable and nonreciprocal single-photon source capable of achieving unconventional photon blockade with high spectral purity.

A. Decoherence effect

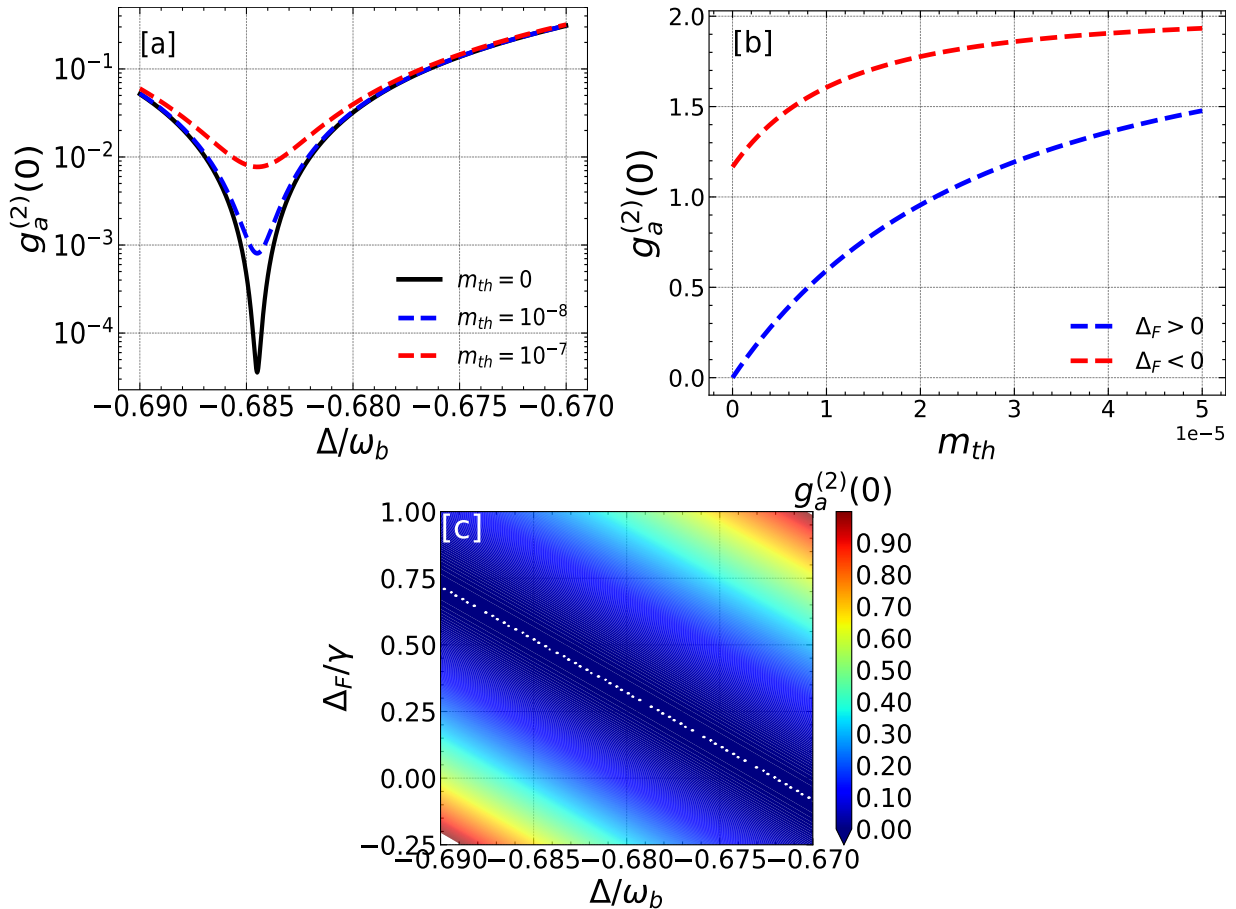


FIG. 3: Plot numerical of the equal-time second-order correlation function $g_a^{(2)}(0)$ versus [a] the normalized detuning Δ/ω_d for different values of m_{th} ; [b] m_{th} for different values of Δ_F with $\lambda = \lambda_{\text{opt}} \approx 2.46 \times 10^{-6}\omega_b$ and $\Delta = \Delta_{\text{opt}} \approx -0.68\omega_b$; and [c] the normalized Δ_F/γ and the normalized detuning Δ/ω_d , where the white dotted line indicates the optimal parameter conditions for unconventional photon blockade (UPB). See the text for value of other parameters.

Figure 3 illustrates the influence of thermal noise in the magnon mode on the photon blockade behavior for both clockwise (CW) and counterclockwise (CCW) spinning directions. In Fig. 3(a), the equal-time second-order correlation function $g_a^{(2)}(0)$ is plotted as a function of the normalized detuning Δ/ω_b for different thermal magnon occupation numbers $m_{\text{th}} = 0$ (black), 10^{-8} (blue), and 10^{-7} (red). As the thermal magnon number increases, the antibunching dip in $g_a^{(2)}(0)$ becomes progressively shallower for both CW and CCW modes, indicating that thermal excitations in the magnon bath weaken the photon blockade. Even a small increase in m_{th} significantly reduces the blockade depth, emphasizing the strong sensitivity of the system to thermal decoherence.

Figure 3(b) presents $g_a^{(2)}(0)$ as a function of the thermal magnon occupation number m_{th} for both $\Delta_F > 0$ and $\Delta_F < 0$, while Fig. 3(c) shows a two-dimensional density plot of $g_a^{(2)}(0)$ versus the normalized detuning Δ/ω_d and the normalized Sagnac shift Δ_F/γ . In both spinning directions, $g_a^{(2)}(0)$ increases with m_{th} , signifying the gradual loss of photon antibunching and the transition toward classical photon statistics. However, for $\Delta_F > 0$, the variation of $g_a^{(2)}(0)$ with m_{th} is relatively slow, which suggests that the CW-driven configuration is slightly more resilient to thermal noise compared with the CCW case. The density plot given in Fig. 3(c) highlights that the strong antibunching occurs only near the optimal combinations of Δ and Δ_F (shown by a white dotted line), whereas any gradual deviations from these values rapidly suppress the photon blockade. Overall, these results demonstrate that thermal magnons play a detrimental role in realizing robust photon blockade, emphasizing the importance of maintaining low magnon temperatures for achieving stable nonreciprocal unconventional photon blockade (UCPB) in a spinning microwave magnomechanical system.

B. $g_a^{(0)}$ versus K and \mathcal{E}

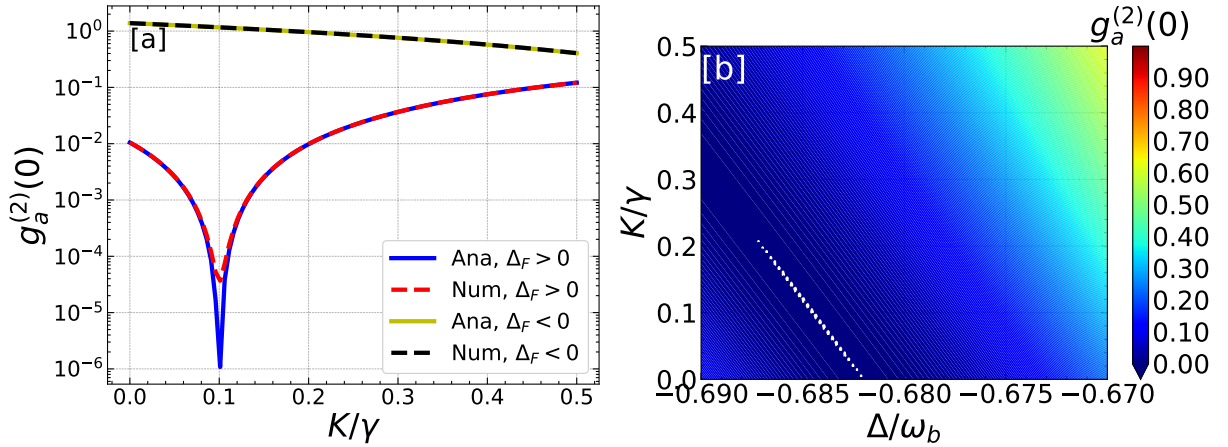


FIG. 4: Plot of the equal-time second-order correlation function $g_a^{(2)}(0)$ parameter versus the normalized Kerr magnon parameter K/γ with $\lambda = \lambda_{\text{opt}} \approx 2.46 \times 10^{-6}\omega_b$ and $\Delta = \Delta_{\text{opt}} = -0.68\omega_b$. Plot numerical of the $g_a^{(2)}(0)$ as a function of the normalized detuning Δ/ω_b and K/γ with $\lambda = \lambda_{\text{opt}} \approx 2.46 \times 10^{-6}\omega_b$, where the white dotted line indicates the optimal parameter conditions for unconventional photon blockade (UPB). See the text for value of other parameters.

The influence of Kerr-type magnon nonlinearity on photon-blockade behavior is analyzed for both clockwise (CW) and counterclockwise (CCW) driving configurations. In Fig. 4(a), the equal-time second-order correlation function $g_a^{(2)}(0)$ is plotted as a function of the normalized Kerr parameter K/γ for four cases: CW-driven mode Analytical (Ana) and Numerical (Num) with $\Delta_F > 0$ (red and sky-blue curves, respectively), and CCW-driven mode Analytical (Ana) and Numerical (Num) with $\Delta_F < 0$ (dark-blue and black curves, respectively). For the CW-driven configuration ($\Delta_F > 0$), the analytical and numerical results overlap almost perfectly and exhibit a very strong photon antibunching minimum at $K/\gamma \approx 0.1$, where $g_a^{(2)}(0) \sim 10^{-6}$, which confirms both the accuracy of the analytical method and the existence of robust unconventional photon blockade (UPB). In contrast, for the CCW-driven configuration ($\Delta_F < 0$), the two curves deviate slightly and show a second pronounced antibunching minimum around $K/\gamma \approx 0.5$, also indicating strong UPB. On gradually changing these optimal nonlinearities, $g_a^{(2)}(0)$ increases again, reflecting the weakening of the photon blockade and the emergence of photon bunching.

A density plot of $g_a^{(2)}(0)$ as a function of both the normalized detuning Δ/ω_b and the Kerr parameter K/γ is shown in Fig. 4(b) for the CCW-driven configuration ($\Delta_F < 0$). The dark-blue regions correspond to strong photon antibunching whereas the white dotted contour marks the optimal parameter conditions for UCPB. The density plot also confirms that strong blockade occurs only within the narrow ranges of detuning and Kerr strength near these optimal points, and deviations from these regions rapidly suppress the photon blockade. These findings demonstrate that Kerr nonlinearity and rotation-induced detuning jointly determine the strength and directionality of the photon-blockade effect, enabling controllable nonreciprocal single-photon emission in the spinning microwave magnomechanical system.

The effect of the driving field amplitude on the photon-blockade behavior is analyzed for both clockwise (CW) and counterclockwise (CCW) driving configurations. In Fig. 5(a), the equal-time second-order correlation function $g_a^{(2)}(0)$ is plotted as a function of the normalized driving field amplitude E/γ at the fixed parameters $\lambda = \lambda_{\text{opt}} \approx 2.46 \times 10^{-6}\omega_b$ and $\Delta = \Delta_{\text{opt}} = -0.68\omega_b$. For

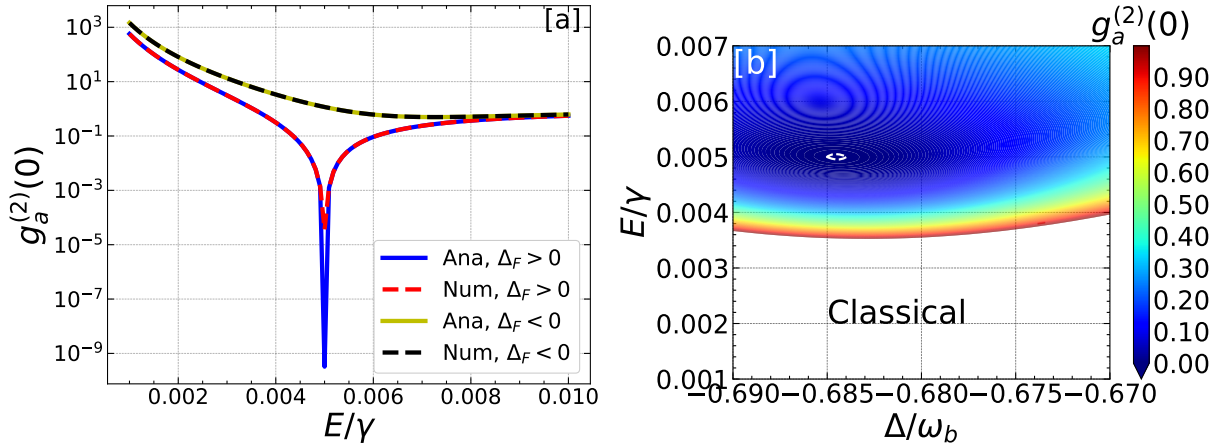


FIG. 5: Plot of the equal-time second-order correlation function $g_a^{(2)}(0)$ parameter versus E/γ with $\lambda = \lambda_{opt} \approx 2.46 \times 10^{-6}\omega_b$ and $\Delta = \Delta_{opt} = -0.68\omega_b$. Plot numerical of the $g_a^{(2)}(0)$ as a function of the normalized detuning Δ/ω_b and E/γ with $\lambda = \lambda_{opt} \approx 2.46 \times 10^{-6}\omega_b$, where the white dotted line indicates the optimal parameter conditions for unconventional photon blockade (UPB). See the text for value of other parameters.

the CW-driven mode ($\Delta_F > 0$), the analytical and numerical results overlap closely and exhibit a very strong photon antibunching minimum at $E/\gamma \approx 0.05$, where $g_a^{(2)}(0) \sim 10^{-6}$, confirming the realization of robust unconventional photon blockade (UPB) under weak excitation. As the driving amplitude increases beyond this range, $g_a^{(2)}(0)$ rises sharply, indicating a transition from strong antibunching to photon bunching due to enhanced multiphoton excitations. For the CCW-driven configuration ($\Delta_F < 0$), a similar trend is observed, but the antibunching occurs at slightly higher E/γ values, showing that the CW mode retains stronger blockade under weaker driving conditions.

A two dimensional density plot of $g_a^{(2)}(0)$ as a function of the normalized detuning Δ/ω_b and the normalized driving field amplitude E/γ is shown in Fig. 5(b). For the CCW-driven configuration ($\Delta_F < 0$), it can be seen that the dark-blue regions denote strong photon antibunching whereas the white dotted contour marks the optimal parameter combinations for UCPB. It is also revealed that pronounced photon blockade occurs for $E/\gamma \geq 0.004$ and within a narrow detuning window around the optimal parameters. It can be seen that outside this range, $g_a^{(2)}(0)$ rapidly increases, and shifts toward white color area, which indicates the classical photon bunching where $g_a^{(2)}(0) \geq 1$. This means that on gradually increasing the driving field amplitude beyond the threshold efficiently activates the destructive quantum interference pathways responsible for photon blockade. So. all these results highlight the crucial role of controlled driving strength for sustaining nonreciprocal single-photon emission in the spinning microwave magnomechanical system.

C. Pure dephasing effects

Since pure dephasing can undermine photon blockade and serve as a source of detrimental decoherence in the system, we investigate its specific impact on the antibunching characteristics of the cavity photons. The effects of pure dephasing are formally modeled by incorporating the following Lindblad term into the master equation:

$$\mathcal{L}_p(\varrho) = \frac{\gamma_p}{2} [2a^\dagger a \varrho a^\dagger a - (a^\dagger a)^2 \varrho - \varrho (a^\dagger a)^2]$$

here, γ_p represents the pure dephasing rate associated with the cavity mode.

The influence of pure dephasing on the photon-blockade characteristics is illustrated in Fig. 6, which presents numerical plots of the equal-time second-order correlation function $g_a^{(2)}(0)$ versus the normalized detuning Δ/ω_b for three pure-dephasing rates γ_p . Panels (a)–(d) correspond to the four optimal parameter sets used previously: (a) and (b) are for $\Delta_F = 0.5\gamma$ (CW mode) with $\lambda_{opt} \approx 2.46157 \times 10^{-6}\omega_b$ and $2.45563 \times 10^{-6}\omega_b$, respectively; (c) and (d) are for $\Delta_F = -0.5\gamma$ (CCW mode) with $\lambda_{opt} \approx 2.46105 \times 10^{-6}\omega_b$ and $2.47275 \times 10^{-6}\omega_b$, respectively. Each panel displays multiple curves for different values of γ_p , permitting a direct assessment of pure-dephasing effects at the same operating point.

Two key insights follow from these plots. First, increasing pure dephasing uniformly weakens the photon blockade: the antibunching minima of $g_a^{(2)}(0)$ become shallower and the values move toward unity (and above), indicating the progressive

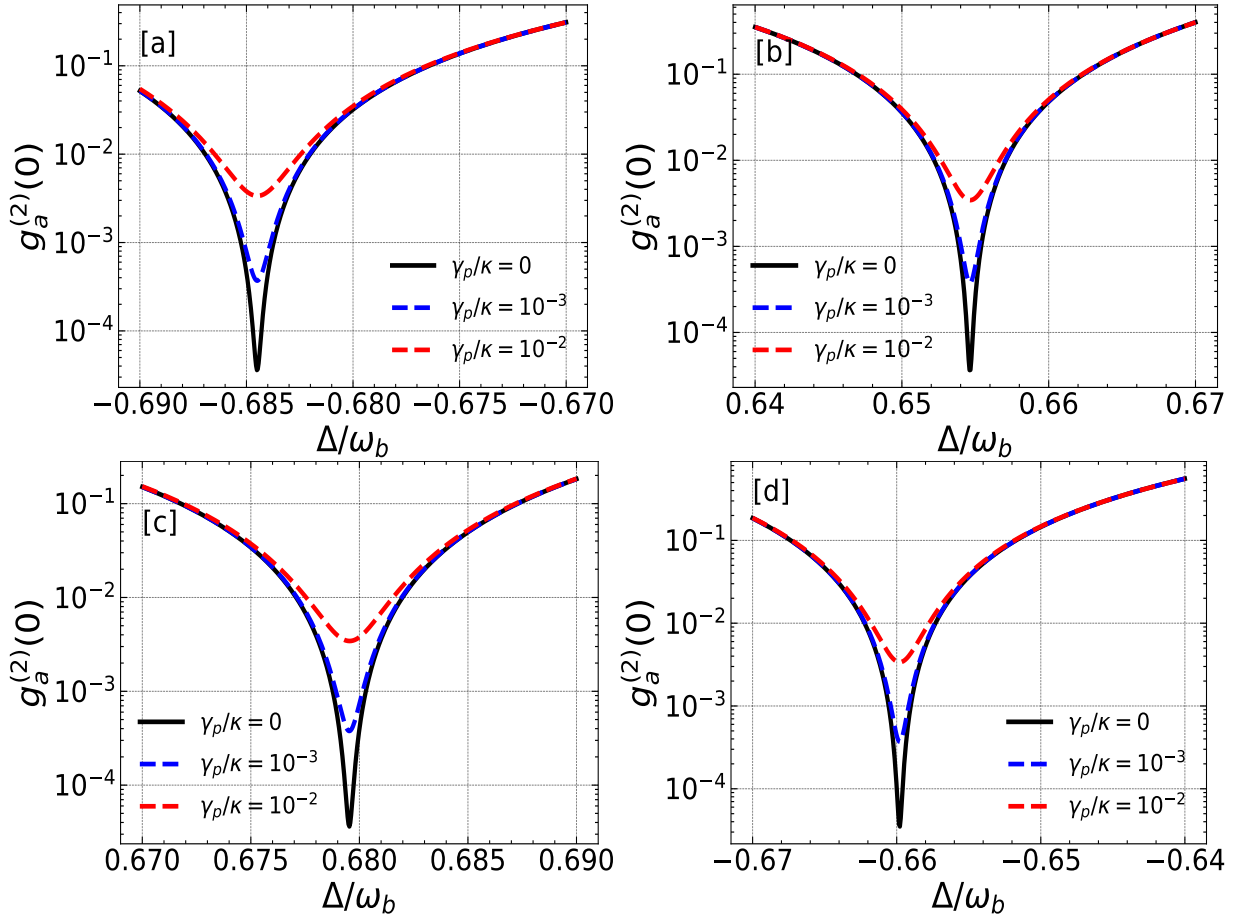


FIG. 6: Plot numerical of the equal-time second-order correlation function $g_a^{(2)}(0)$ versus the normalized detuning Δ/ω_b for different values of pure-dephasing rates γ_p with $\lambda = \lambda_{opt} \approx (2.46, 2.46, 2.46 \text{ and } 2.47) \times 10^{-6}\omega_b$ in (a), (b), (c) and (d), respectively. $\Delta_F = 0.5\gamma$ in (a-b) and $\Delta_F = -0.5\gamma$ in (c-d). See the text for value of other parameters.

loss of nonclassical correlations. Second, the degree of robustness depends both on the chosen optimal pair $(\Delta_{opt}, \lambda_{opt})$ and on the driving direction. For $\Delta_F = 0.5\gamma$ (panels a–b), the antibunching minimum survives for small γ_p but is visibly reduced for larger dephasing. For the $\Delta_F = -0.5\gamma$ panels ((c),(d)), corresponding to the CCW-driven configuration, increasing γ_p similarly weakens the blockade, yet the antibunching dip remains comparatively more robust for certain optimal λ_{opt} values, persisting even at higher dephasing rates. Overall, these results demonstrate that moderate pure dephasing does not immediately destroy unconventional photon blockade (UCB) as small γ_p values only reduce its depth, whereas stronger dephasing rate drives $g_a^{(2)}(0)$ toward or above unity, marking a transition from quantum to classical photon statistics.

D. Non-classicality : Mandel Q

To characterize the statistical properties of the photon, we introduce the Mandel Q parameter, as discussed in Ref. [77]

$$Q_a := \frac{\text{Tr}(\varrho_s a^\dagger a^2) - [\text{Tr}(\varrho_s a^\dagger a)]^2}{\text{Tr}(\varrho_s a^\dagger a)}, \quad (22)$$

A negative value of Q_a ($Q_a < 0$) indicates quantum statistical properties for the photon mode, whereas a non-negative value ($Q_a \geq 0$) indicates classical properties.

The Mandel parameter Q_a quantifies deviations from Poissonian photon statistics which means the negative values ($Q_a < 0$) correspond to sub-Poissonian, nonclassical light exhibiting photon antibunching, whereas $Q_a \geq 0$ denotes Poissonian or super-Poissonian (classical or bunched) statistics. Both subplots of Figure 7 correspond to the CCW-driven configuration ($\Delta_F = -0.5\gamma$) with the optimal coupling $\lambda_{opt} \approx 2.46 \times 10^{-6}\omega_b$.

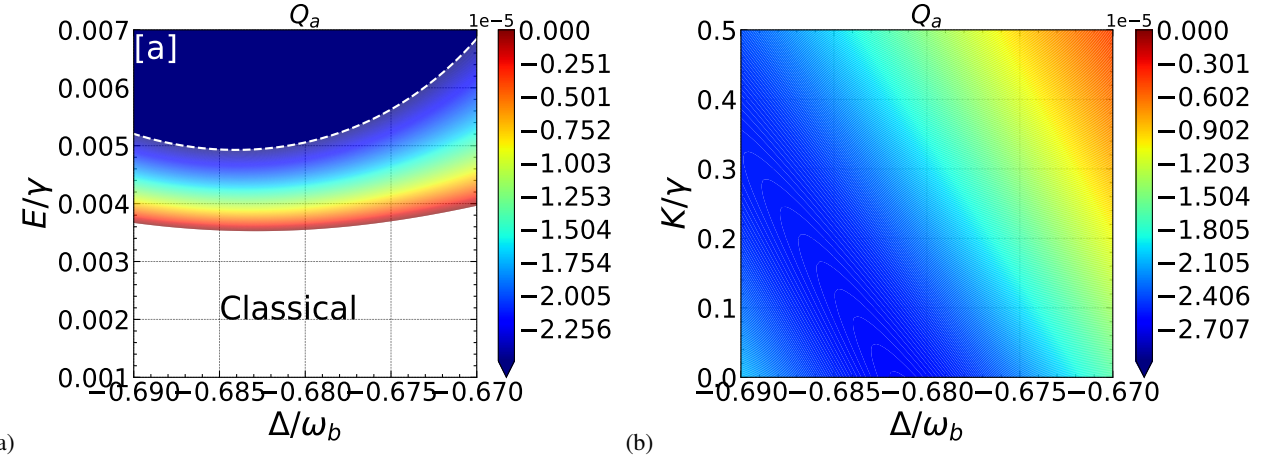


FIG. 7: Plot numerical of the Mandel Q_a parameter versus the normalized detuning Δ/ω_b and: K/γ in [a] and amplitude of probe field E/γ in [b] with $\lambda = \lambda_{opt} \approx 2.46 \times 10^{-6} \omega_b$ and $\Delta_F = -0.5\gamma$. See the text for value of other parameters.

Figure 7(a) shows Q_a as a function of the normalized detuning Δ/ω_b and the driving field amplitude E/γ . A pronounced dark-blue region with $Q_a < 0$ appears for $E/\gamma \geq 0.005$ near the optimal detuning, revealing strong sub-Poissonian photon statistics consistent with unconventional photon blockade (UCPB). The white dotted line indicates the optimal parameter combinations where destructive quantum interference maximizes photon blockade whereas outside this narrow region, Q_a approaches towards zero, signifying a transition to classical photon bunching.

Figure 7(b) presents Q_a as a function of the normalized detuning Δ/ω_b and the Kerr nonlinearity K/γ . It can be seen that the negative- Q_a regions are observed around $K/\gamma \approx 0.5$ and near the same optimal detuning, confirming that photon blockade generation is highly sensitive to both Kerr strength and detuning. The white or light-coloured regions in both subplots correspond to Q_a approaching towards zero which indicate classical photon statistics. Overall, the Mandel parameter behavior very closely parallels that of $g_a^{(2)}(0)$ which means that regions with $Q_a < 0$ coincide with $g_a^{(2)}(0) < 1$, confirms that both consistently identify the unconventional photon-blockade regime and its dependence on driving amplitude, Kerr nonlinearity strengths, and cavity detuning in the spinning microwave magnomechanical system.

E. $g^{(0)}$ vs τ and time

The second-order correlation function, $g_a^{(2)}(\tau)$, is a significant quantity for characterizing the statistical properties of the photons. It represents the joint probability of detecting a photon at time t and a second photon at time $t + \tau$ (up to a proportionality constant), and its time evolution is calculated as

$$g_a^{(2)}(\tau) = \frac{\langle a^\dagger(t)a^\dagger(t + \tau)a(t + \tau)a(t) \rangle}{\langle a^\dagger(t)a(t) \rangle^2} \quad (23)$$

The condition $g_a^{(2)}(\tau) > g_a^{(2)}(0)$ for delay times $\tau > 0$ provides evidence of photon blockade and confirms the sub-Poissonian statistics of the emitted photons. We note that $g_a^{(2)}(\tau)$ grows with increasing τ , eventually reaching its maximum value (unity) near $\tau \approx 3.5 \mu\text{s}$, as illustrated in Figure 8 (a-d). Furthermore, $g_a^{(2)}(\tau)$ increases until it reaches its maximum value of unity (characteristic of a coherent state) at $\tau \approx 3.5 \mu\text{s}$ (the approximate lifetime of the photons in the cavity), as shown in Figure 8 (a-d). This indicates that as the time delay increases, the photons eventually become statistically independent (coherent).

V. CONCLUSION

In summary, we realize nonreciprocal unconventional photon blockade in a spinning microwave cavity magnomechanical system. This is made possible by combining the nonlinear effects from Kerr-magnon interactions and a degenerate optical parametric amplifier under weak pump driving. The rotation-induced Sagnac–Fizeau shift plays a key role in enabling the directional photon blockade, as confirmed through both analytical theory and numerical simulation. Our results show that the effect remains highly robust against thermal noise, and we examine how the probe field amplitude and magnetic-dipole coupling

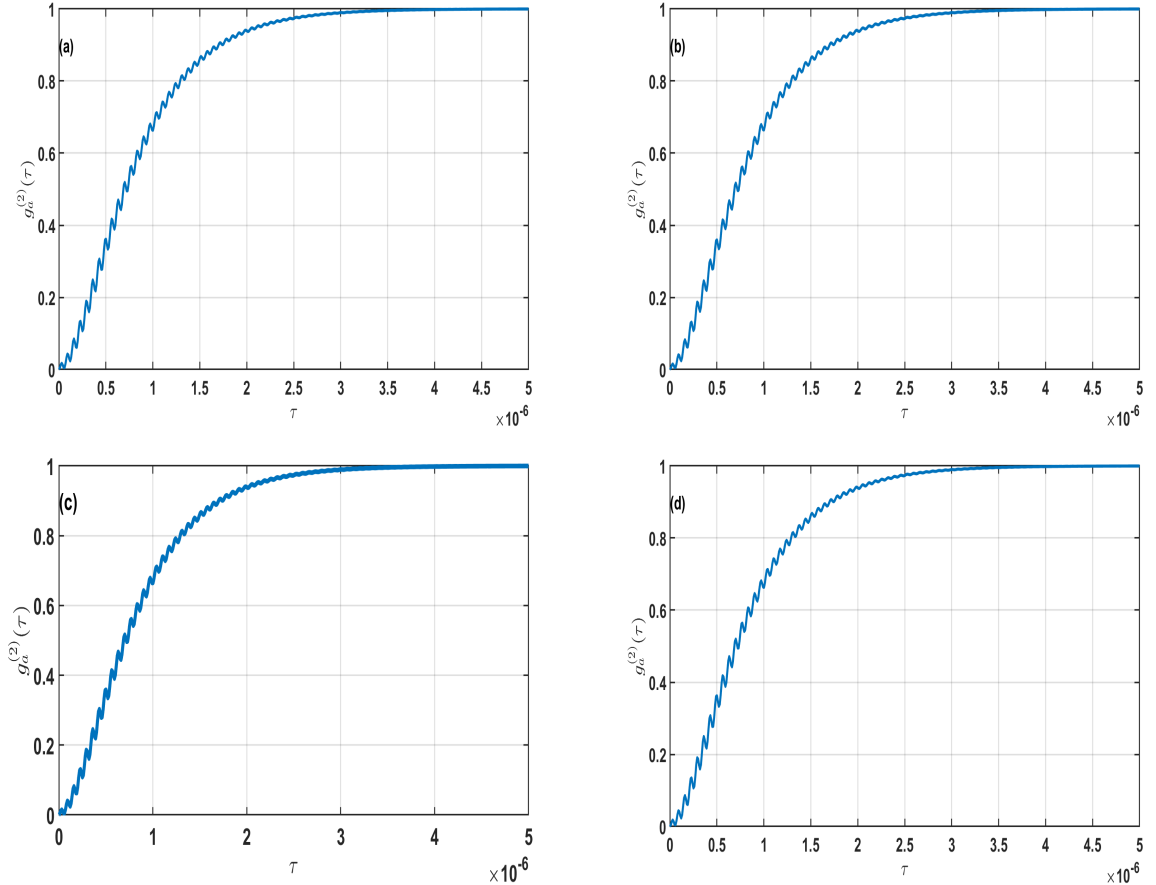


FIG. 8: Time evolution of the second-order correlation function, $g_a^{(2)}(\tau)$ ($t = 0$) with $\Delta = +0.5\gamma$ in (a) and (b) with $\lambda = 2.45563 \times 10^{-6}\omega_b$ and $\lambda = 2.46157 \times 10^{-6}\omega_b$, respectively. And $\Delta = -0.5\gamma$ in (c) and (d) with $\lambda = 2.46105 \times 10^{-6}\omega_b$ and $\lambda = 2.47275 \times 10^{-6}\omega_b$, respectively. See the text for value of other parameters.

strength influence the system response. We also demonstrate the nonclassical behavior of the magnon and photon modes using the Mandel parameter, along with the time-delay second-order correlation function. Overall, this work offers a promising pathway toward implementing direction-dependent single-photon sources and advancing integrated quantum technologies in spinning cavity-magnonic systems.

[1] V. Giovannetti, S. Lloyd, and L. Maccone, *Nat. Photonics* **5**, 222 (2011).
[2] K. Stannigel *et al.*, *Phys. Rev. Lett.* **109**, 013603 (2012).
[3] C. H. Bennett and D. P. DiVincenzo, *Nature* **404**, 247 (2000).
[4] I. Buluta, S. Ashhab, and F. Nori, *Rep. Prog. Phys.* **74**, 104401 (2011).
[5] A. Faraon *et al.*, *Nat. Phys.* **4**, 859 (2008).
[6] K. M. Birnbaum *et al.*, *Nature* **436**, 87 (2005).
[7] A. Reinhard *et al.*, *Nat. Photonics* **6**, 93 (2012).
[8] K. Müller *et al.*, *Phys. Rev. Lett.* **114**, 233601 (2015).
[9] C. Hamsen *et al.*, *Phys. Rev. Lett.* **118**, 133604 (2017).
[10] C. M. Zheng *et al.*, *New J. Phys.* **25**, 043030 (2023).
[11] C. Lang *et al.*, *Phys. Rev. Lett.* **106**, 243601 (2011).
[12] A. J. Hoffman *et al.*, *Phys. Rev. Lett.* **107**, 053602 (2011).
[13] C. Vaneph *et al.*, *Phys. Rev. Lett.* **121**, 043602 (2018).
[14] H. J. Snijders *et al.*, *Phys. Rev. Lett.* **121**, 043601 (2018).
[15] C. Sayrin *et al.*, *Phys. Rev. X* **5**, 041036 (2015).

- [16] L. Tang *et al.*, Phys. Rev. A **99**, 043833 (2019).
- [17] A. Kamal, J. Clarke, and M. H. Devoret, Nat. Phys. **7**, 311 (2011).
- [18] D. L. Sounas and A. Alù, Nat. Photonics **11**, 774 (2017).
- [19] A. Ø. Svela *et al.*, Light Sci. Appl. **9**, 204 (2020).
- [20] Y. F. Jiao *et al.*, Phys. Rev. Lett. **125**, 143605 (2020).
- [21] Y. F. Jiao *et al.*, Phys. Rev. Appl. **18**, 064008 (2022).
- [22] Y. L. Ren, Opt. Lett. **47**, 1125 (2022).
- [23] J. Chen *et al.*, Phys. Rev. B **108**, 024105 (2023).
- [24] Y. Jiang *et al.*, Phys. Rev. Appl. **10**, 064037 (2018).
- [25] Y. Xu *et al.*, Phys. Rev. A **103**, 053501 (2021).
- [26] Y. Tabuchi, S. Ishino, T. Ishikawa, R. Yamazaki, K. Usami, and Y. Nakamura. Phys. Rev. Lett. **113**, 083603 (2014).
- [27] Jie Li, S-Y Zhu and G. S. Agarwal. Phys. Rev. Lett. **121**, (2018) 203601.
- [28] Y. Mei, H. Shen and Jie Li. Phys. Rev. Lett. **124**, (2020) 213604.
- [29] X. Zhang, C. L. Zou, L. Jiang, and H. X. Tang. Sci. Adv. **2**, e1501286 (2016).
- [30] Y. Tabuchi, S. Ishino, A. Noguchi, T. Ishikawa, R. Yamazaki, K. Usami, and Y. Nakamura. Science, **349**(6246), 405-408 (2015).
- [31] D. Lachance-Quirion, S. P. Wolski, Y. Tabuchi, S. Kono, K. Usami, and Y. Nakamura. Science **367**.6476 (2020) 425-428.
- [32] M. Amazioug, B. Teklu and M. Asjad. Scientific Reports **13**.1 (2023) 3833.
- [33] M. Amazioug, S. K. Singh, B. Teklu and M. Asjad. Entropy **25**.10 (2023) 1462.
- [34] M. Amazioug, J.-X. Peng, D. Dutykh, M. Asjad, Eur. Phys. J. Plus **140** (2025) 132.
- [35] F. H. Mathkoor, S. K. Singh, R. Ahmed, J. X. Peng, M. Amazioug, M. Khalid and A. Sohail. Scientific Reports, **15**(1), 13503 (2025).
- [36] M. Asjad, J. Li, S. Y. Zhu and J. Q. You. Fundamental Research, **3**(1) (2023) 3-7.
- [37] M. Amazioug, D. Dutykh, B. Teklu and M. Asjad. Annalen der Physik **536**.4 (2024) 2300357.
- [38] X. Deng, K. K. Zhang, T. Shui and W. X. Yang. Physical Review A, **110**(6) (2024) 063711.
- [39] R. Hou, W. Zhang, X. Han, H. F. Wang and S. Zhang. Scientific Reports, **15**(1) (2025) 5145.
- [40] P. C. Ge, Y. Yu, H. T. Wu, X. Han, H. F. Wang, and S. Zhang. Scientific Reports, **15**(1) (2025) 7937.
- [41] W. Zhang, S. Liu, S. Zhang, H. F. Wang. Optics Express, **33**(2) (2025) 3339-3349.
- [42] R. Huang, A. Miranowicz, J.-Q. Liao, F. Nori, and H. Jing, Phys. Rev. Lett. **121**, 153601 (2018).
- [43] M. Amghar and M. Amazioug. Optik **311** (2024) 171940
- [44] C. O. Edet, M. Asjad, D. Dutykh, N. Ali and O. Abah. Physical Review Research, **6**(3) (2024) 033037.
- [45] X. Deng, K. K. Zhang, T. Shui, W. X. Yang, Phys. Rev. A **2024**, **110**, 063711.
- [46] M. S. Ebrahimi and M. B. Harouni. Journal of Physics B: Atomic, Molecular and Optical Physics, **56**(23), 235501 (2023).
- [47] I. M. Mirza *et al.*, Opt. Express **27**, 25515 (2019).
- [48] M. Peng *et al.*, Phys. Rev. A **107**, 033507 (2023).
- [49] B. Li *et al.*, Phys. Rev. A **103**, 053522 (2021).
- [50] R. Huang *et al.*, Phys. Rev. Lett. **121**, 153601 (2018).
- [51] K. Wang *et al.*, Phys. Rev. A **100**, 053832 (2019).
- [52] H. Z. Shen *et al.*, Phys. Rev. A **101**, 013826 (2020).
- [53] X. W. Xu *et al.*, Phys. Rev. Appl. **13**, 044070 (2020).
- [54] X. Shang *et al.*, Laser Phys. Lett. **18**, 115202 (2021).
- [55] Y. M. Liu *et al.*, Opt. Express **31**, 12847 (2023).
- [56] B. Li *et al.*, Photonics Res. **7**, 630 (2019).
- [57] Y. M. Liu *et al.*, Phys. Rev. A **107**, 063701 (2023).
- [58] W. Zhang *et al.*, Sci. China Phys. Mech. Astron. **66**, 240313 (2023).
- [59] W. S. Xue *et al.*, Opt. Lett. **45**, 4424 (2020).
- [60] Y. W. Jing *et al.*, Phys. Rev. A **104**, 033707 (2021).
- [61] H. Xie *et al.*, Phys. Rev. A **106**, 053707 (2022).
- [62] C. Kittel, Phys. Rev. **73**, 155 (1948).
- [63] X. Zhang *et al.*, Phys. Rev. Lett. **113**, 156401 (2014).
- [64] H. Huebl *et al.*, Phys. Rev. Lett. **111**, 127003 (2013).
- [65] L. Bai *et al.*, Phys. Rev. Lett. **114**, 227201 (2015).
- [66] T. J. Kippenberg *et al.*, Phys. Rev. Lett. **95**, 033901 (2005).
- [67] W. Zhao *et al.*, Sci. China Phys. Mech. Astron. **63**, 224211 (2020).
- [68] Z. B. Yang *et al.*, Ann. Phys. (Berlin) **532**, 2000196 (2020).
- [69] Collett M J and Gardiner C W 1984 Phys. Rev. A **30** 1386
- [70] Agarwal G S 2006 Phys. Rev. Lett. **97** 023601
- [71] He W P and Li F L 2007 Phys. Rev. A **76** 012328
- [72] Yan Z H, Jia X J, Su X L, Duan Z Y, Xie C D and Peng K C 2012 Phys. Rev. A **85** 040305
- [73] Chen H X and Zhang J 2009 Phys. Rev. A **79** 063826
- [74] Shang Y N, Jia X J, Shen Y M, Xie C D and Peng K C 2010 Opt. Lett. **35** 853
- [75] R. Hou, W. Zhang, X. Han, H. F. Wang and S. Zhang. Scientific Reports, **15**(1) (2025) 5145
- [76] Zhou Y Y, Jia X J, Li F, Yu J, Xie C D and Peng K C 2015 Scientific Reports **5** 11132
- [77] Z. Liang, Y. Wu, J. Li, Opt. Lett. **2024**, **49**, 2749.